MICROSTRUCTURE-BASED EVALUATION OF THE FATIGUE BEHAVIOUR OF RAILWAY WHEEL STEELS

F. Walther & D. Eifler
Institute of Materials Science and Engineering
University of Kaiserslautern, P. O. Box 3049, D-67653 Kaiserslautern, Germany

ABSTRACT

Current investigations concentrate on the relation between the microstructural gradients in the wheel rim and tire cross-sections and the depending local fatigue behaviour. The microstructural gradients are a consequence of the industrial heat treatment and the size of the components. The specimens were machined from defined depth positions from original monobloc wheels and tires of the UIC-qualities R7/B6 (UIC: International Railway Union). Stress- and total-strain-controlled experiments were performed on servo-hydraulic testing systems to determine cyclic deformation, stress-strain and S,N-curves. In addition to mechanical stress-strain (σ,ε) hysteresis measurements, the changes of the specimen temperature ΔT and voltage ΔU due to plastic deformation processes were regarded. The measured values are based on physical processes and therefore show a strong interrelation with the underlying fatigue process. The substitution of the plastic strain amplitude $\varepsilon_{a,p}$ by ΔT or ΔU leads to cyclic stress-temperature- (σ_a,ΔT-) or stress-voltage- (σ_a,ΔU-) curves, according to Morrow. ΔT and ΔU can also be used similar to $\varepsilon_{a,p}$ for a lifetime prediction according to Manson/Coffin. Additionally with these data S,N-curves can be specified according to Basquin. Light, scanning and transmission electron microscopy allow to interpret the measured physical data using the microstructural details.

1 INTRODUCTION

Due to changing traffic requirements the development of new railway vehicle generations with new materials, constructions and manufacturing methods aims at a higher efficiency in respect of weight and energy consumption. For safety parts, in particular railway wheels, a reliable design in consideration of mechanical and thermal aspects as well as sufficient testing is essential. As a consequence of higher speeds in passenger and higher axle loads in freight traffic a substantial increase of the complex service loading of the wheels has to be considered. Currently the dimensioning of wheels was realized according to standards for calculation and construction described in the admission procedure, e.g. UIC 510-5 or the draft of DIN-EN-13262-1. The available material data are the base of a loading-adequate construction. Therefore the optimization of the wheel/rail-system requires a detailed knowledge of the fatigue behaviour of the highly loaded railway wheel steels (e.g. Sakamoto [1], Liu [2], Ekberg [3]).

Since for wheel steels only a few systematic investigations of the fatigue behaviour are available so far, the actual investigations concentrate on the relation between the local microstructure and the description of the depending fatigue processes. The fatigue behaviour is characterized and evaluated by stress-strain (σ,ε) hysteresis as well as thermometrical and electrical measurements. The changes of temperature ΔT and voltage ΔU yield integral signals from the tested material volume and are complementary to the plastic strain amplitude $\varepsilon_{a,p}$. The microstructural characterization of the different material conditions was done by light (LM), scanning (SEM) and transmission (TEM) electron microscopy, together with digital image processing.

2 MATERIALS

The investigations were performed with specimens machined from the wheel rim and tire cross-sections of original monobloc wheels R7 and tires B6 corresponding to the UIC-specifications 812-3 V and 810-1 V. Table 1 contains the chemical compositions.

Table 1. Chemical composition (wt. %) of wheels R7 and tires B6

ELEMENTS	**C**	**Si**	**Mn**	**Cr**	**Cu**	**Mo**	**Ni**
R7	0.53	0.32	0.75	0.26	0.04	0.01	0.11
B6	0.62	0.44	0.76	0.21	0.03	0.01	0.03

Characteristic SEM-micrographs with ferritic-pearlitic structures of the wheel and tire steels are shown in Figs. 1a and b. Beside the significant higher ferrite portion of the wheel steel, the ferrite areas and cementite lamellae could be identified. In separate micrographs etched according to Le Pera it was proved, that no martensitic or bainitic phases exist in the tire material.

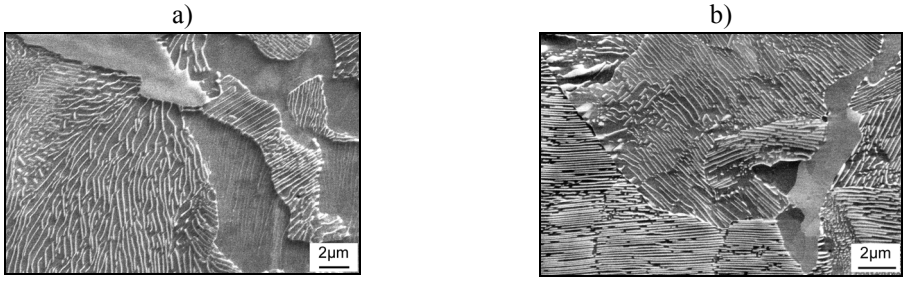

Figure 1: SEM-microstructures of R7 (a) and B6 (b)

As a consequence of the industrial heat treatment and the size of complete wheels and tires with a weight of about 400 kg microstructural gradients occur. In contrast to tires B6, the quenching process of wheels R7 with a fine-dispersed liquid is limited to the tread. As a result, the ferrite portion increases continuously from the outer wheel rim towards the disc and flange with increasing tread distance (Fig. 2a). The differences in the ferrite content of tires B6 are less pronounced with maximum values of 2 area-% in the centre of the cross-section (Fig. 2b) (Walther [4]).

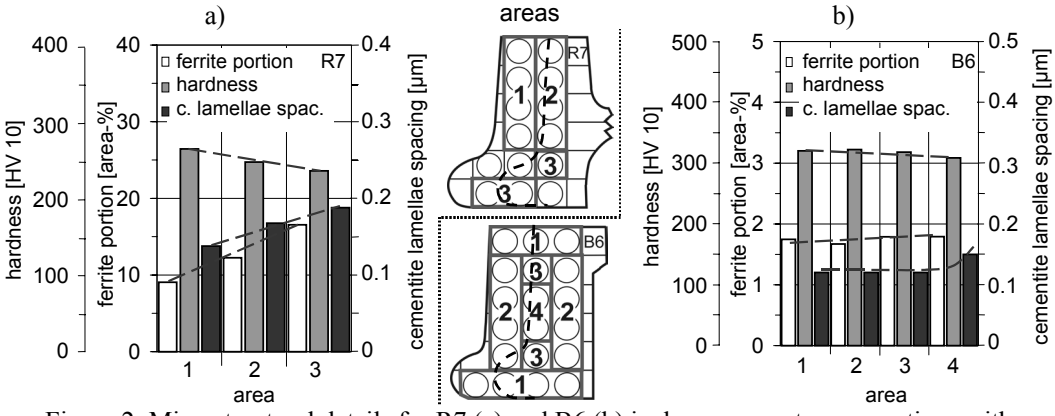

Figure 2: Microstructural details for R7 (a) and B6 (b) incl. component cross-sections with specimen positions and area classifications

Beside the ferrite portion and distribution, the fatigue behaviour is also determined by the spacing of the cementite lamellae. Qantitatively analysed SEM-micrographs show position-dependent spacings of 0.14-0.19 µm (R7) and 0.12-0.15 µm (B6). Equivalent to the ferrite portion, highest cementite lamellae spacings occur in interior sections of the components with smaller cooling rates, corresponding to the continuous time-temperature-transformation diagram. Vickers hardness measurements could be quantitatively correlated with the ferrite portions and the cementite lamellae spacings.

For an exact specification of the fatigue behaviour 14 (R7) resp. 19 (B6) specimens were machined from defined depth positions, according to the circles in the cross-section drawings (Fig. 2). The wear limit of about 25-35 mm below the tread is marked by a broken line. Due to corresponding microstructural details and cyclic deformation curves (see chapt. 4), the specimen positions per cross-section can be arranged in 3 areas (Ai) (R7: A1⇨A3) resp. 4 areas (B6: A1⇨A4) of comparable microstructural and cyclic characteristics.

3 EXPERIMENTAL PROCEDURES

Stress- and total-strain-controlled experiments were performed at the load ratio R=-1 on servo-hydraulic testing systems at ambient temperature with a frequency of 5 Hz and triangular load-time functions. The tests were finished by failure or after reaching $2 \cdot 10^6$ cycles. The characterization of the fatigue behaviour is done by recording mechanical (σ,ε) hysteresis loops. With thermocouples fixed in the gauge length additional information (ΔT) about microstructural processes can be detected. Apart from the geometry, the electrical resistance and consequently the voltage ΔU is a function of the specific electrical resistance, which is directly influenced by the defect structure of a cyclically loaded component. During the experiments a direct-current power supply providing 8 A is fixed at both specimen shafts. Two wires are spot welded at the transitions between the gauge length and the shafts to measure the potential (Schelp [5]). The experiments yield characteristic cyclic deformation, temperature and voltage curves corresponding to the actual fatigue state of railway wheels.

4 RESULTS

Subsequent to load increase tests to identify critical stress amplitudes and to estimate the endurance limit, the stress amplitudes σ_a=400 MPa (R7) and 500 MPa (B6) were selected to characterize the local fatigue behaviour in detail. Generally, the fatigue behaviour shows a strong dependence on the individual microstructure (cf. Fig. 2). Compared to specimens of homogeneous normalized medium carbon steels with similar chemical compositions, e.g. SAE 1045, significant quantitative differences are present. With increasing tread distance and according increasing ferrite portions resp. cementite lamellae spacings (B6) maximum values of $\varepsilon_{a,p}$, ΔT and ΔU after shorter incubation intervals lead to decreasing lifetimes N_f.

In Fig. 3a, ΔT is plotted versus N for the different specimen positions of B6 at σ_a=500 MPa. The 19 cyclic deformation curves could be combined to 4 characteristic area-specific arrays of curves. A macroscopic quasi-elastic incubation interval is followed by cyclic softening, reaching maximum values at approx. 5% N_f. Then cyclic hardening with decreasing values extends to the macroscopic crack growth. Maximum ΔT-values up to 30 K are present in the cross-section centre (area 4 (A4), cf. Fig. 2). In the flange and the opposite side (A1) ΔT_{max}=5 K allows a 20 times longer lifetime up to $4 \cdot 10^5$ cycles.

In Fig. 3b, the cycle-dependent development of $\varepsilon_{a,p}$, ΔT and ΔU is shown as f(N) for specimens of the B6-tread (A2). Equivalent to ΔT, cyclic softening (hardening) causes an analogous increase (decrease) of $\varepsilon_{a,p}$ and ΔU. The measured values are based on physical processes and therefore show a strong interrelation with the underlying fatigue process, leading to similar curves. This

confirms, that the deformation-induced microstructural changes can be described in a definite and comparable manner by the plastic strain amplitude and the changes of temperature and voltage.

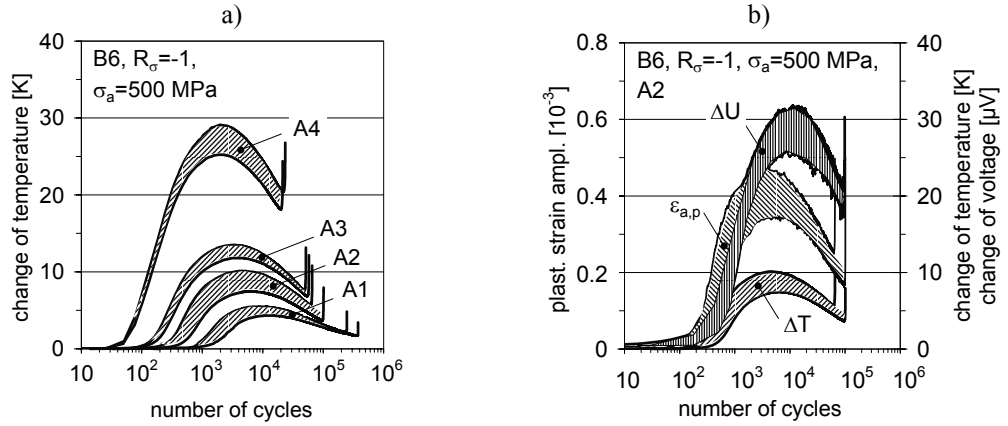

Figure 3: Cyclic temperature curves of B6 (a) and interrelation of $\varepsilon_{a,p}$, ΔT and ΔU for the B6-tread

Figure 4a presents the relation of the plastic strain amplitude at $N_f/2$, the lifetime and the ferrite portion for specimens of R7 at σ_a=400 MPa. An increasing ferrite portion leads to increasing plastic strain amplitudes from smallest $\varepsilon_{a,p}$-values in the tread towards $1.8 \cdot 10^{-3}$ in the flange (A1⇨A3) combined with a substantial decrease in the lifetime from $1.34 \cdot 10^5$ to $0.14 \cdot 10^5$. The development of $\varepsilon_{a,p}$ and N_f as function of the microstructure is mathematically described in the diagram.

In addition, stress-controlled experiments with amplitudes in the range 320 MPa ≤ σ_a ≤ 480 MPa (R7) resp. 380 MPa ≤ σ_a ≤ 580 MPa (B6) were performed in cross-sections of comparable fatigue behaviour for the determination of cyclic deformation, stress-strain (Fig. 4b) and S,N-curves (Fig. 5a).

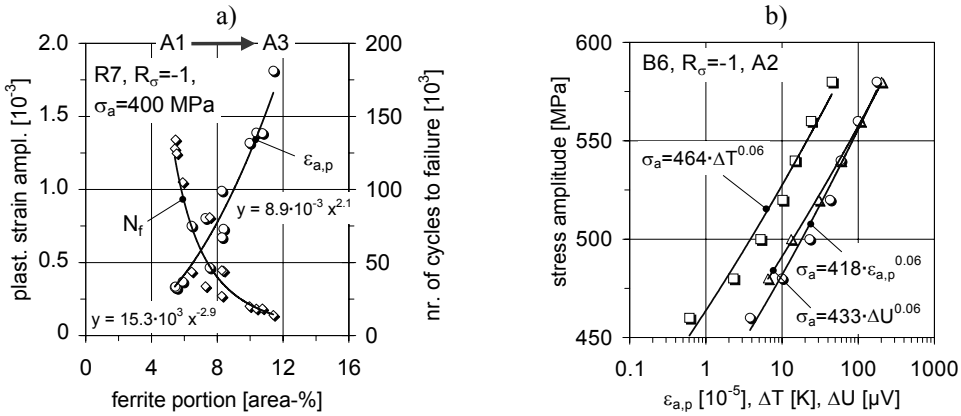

Figure 4: Relation of $\varepsilon_{a,p}$, N_f and ferrite portion for R7 (a) and CSS-, CST- and CSU-curves for the B6-tread (b)

The substitution of $\varepsilon_{a,p}$ by ΔT or ΔU leads to cyclic stress-temperature (CST-) and stress-voltage (CSU-) curves, as shown in Fig. 4b for stress-controlled experiments in the tread of B6. The pairs of measured data were taken at $N_f/2$. Due to identical exponents in the modified descriptions ac-

cording to the power law of Morrow, the fitting lines are shifted nearly parallel to each other. The measured values are equivalently suitable for the assessment of the fatigue behaviour.

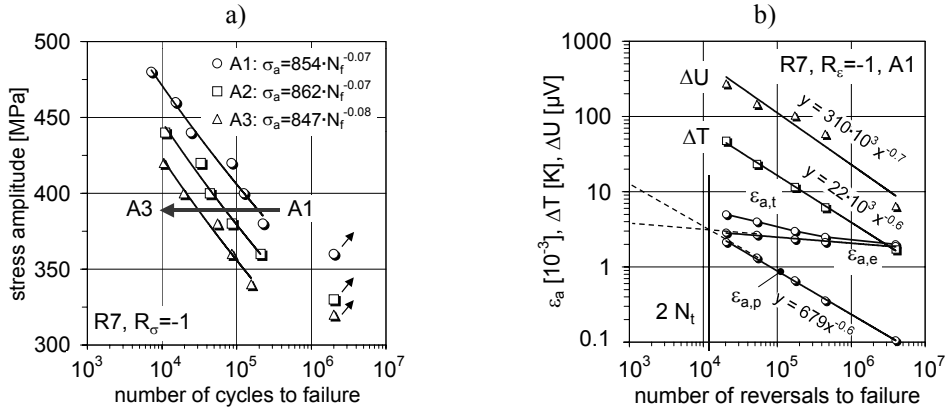

Figure 5: Area-specific S,N-curves of R7 (a) and Manson-Coffin-diagram for the R7-tread (b)

The relation between σ_a and N_f is presented according to Basquin in Fig. 5a for R7. The increasing ferrite portion (A1⇨A3) shifts the area-specific Woehler curves to shorter lifetimes. With stress amplitudes of 320 MPa (A3), 330 MPa (A2) and 360 MPa in A1 $2 \cdot 10^6$ cycles are reached without failure. This S,N-diagram illustrates impressively the strong dependence between the local microstructure and the corresponding lifetime.

Beside total strain amplitudes in the range $1.5 \cdot 10^{-3} \leq \varepsilon_{a,t} \leq 5 \cdot 10^{-3}$ in Fig. 5b, the relationship of $\varepsilon_{a,p}$, ΔT and ΔU at $N_f/2$ versus the number of reversals to failure is shown according to Manson-Coffin for the tread of R7. The nearly parallel fitting lines of the physical variables $\varepsilon_{a,p}$, ΔT and ΔU can also be used for a qualified description of fatigue processes under total strain control. For both materials, with increasing ferrite portion resp. cementite lamellae spacing the transition number of cycles N_t ($\varepsilon_{a,p}$ = elastic strain amplitude $\varepsilon_{a,e}$) is shifted to higher values.

Figure 6a clarifies the relation of the plastic strain amplitude and the dislocation density exemplarily for R7- (σ_a=400 MPa) and B6-specimens (σ_a=500 MPa) of the tread. As mentioned before, for both materials maximum values of $\varepsilon_{a,p}$, ΔT and ΔU occur in the state of cyclic softening at approx. 5% N_f and decrease in the state of cyclic hardening (observed at 85% N_f). Changing cyclic properties are mainly due to the development of the density and arrangement of dislocations. The determination of the dislocation densities by X-ray diffraction and TEM-investigations were performed at the University of Mining and Technology, Freiberg, Germany.

The virgin state (0% N_f) of R7 (Fig. 6b) is characterized by subgrain-structures (5 µm) in the ferrite (∅ 10-20 µm). With σ_a=400 MPa at 5% N_f within the ferrite, stretched and partly veins-like cells are present. The following cyclic hardening is combined with a considerable reduction of the cell sizes to 2-3 µm. In B6-specimens at 5% N_f no vein or cell structures could be found in the ferrite grains (∅ 5-10 µm). Loading with σ_a=500 MPa until 85% N_f leads to cell diameters of 0.3-0.5 µm. For both materials, three-dimensional cell structures are present in the ferrite in the cyclic hardening state and in less number in the ferrite lamellae of the pearlite. The appropriate dislocation densities increase for R7 from $6.2 \cdot 10^9$ cm^{-2} (0% N_f) to $7.7 \cdot 10^9$ cm^{-2} (5% N_f) and for B6 from $1.2 \cdot 10^9$ cm^{-2} to $3.5 \cdot 10^9$ cm^{-2} (Fig. 6a). Areas with higher ferrite portion (e.g. R7, A3) resp. cementite lamellae spacing (e.g. B6, A4) are characterized by smaller dislocation densities. Generally, in B6 they are 2-3 times smaller compared to R7.

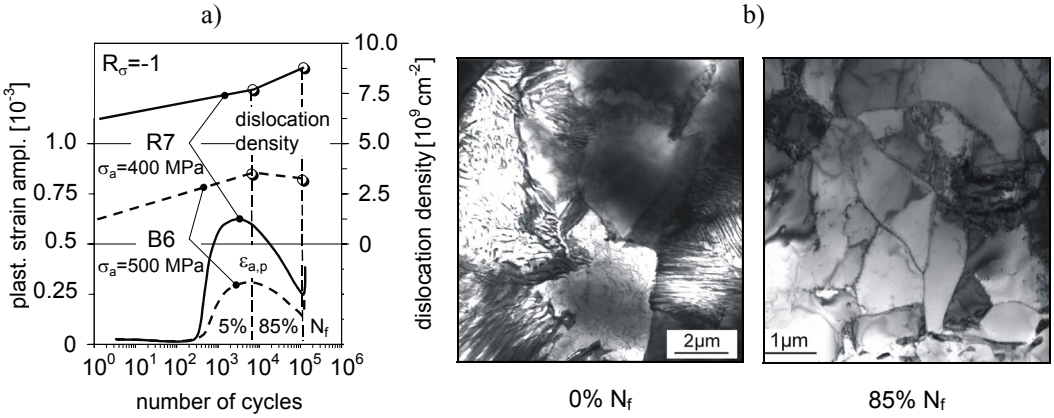

Figure 6: Relation of $\varepsilon_{a,p}$ and dislocation density for R7 and B6 (a) and TEM-micrographs of R7 (σ_a=400 MPa)

5 CONCLUSIONS

Due to the industrial heat treatment and their size, the rim of railway wheels R7 and the cross-section of tires B6 are characterized by microstructures with position-dependent ferrite portions and cementite lamellae spacings. The influence of the microstructural gradients on the fatigue behaviour is of great practical relevance. Subsequent to incubation intervals more or less pronounced cyclic softening and hardening processes occur during cyclic loading of specimens machined from defined depth positions from original UIC-components. Beside the plastic strain amplitude, temperature and voltage measurements are suitable techniques to describe deformation-induced microstructural changes in a definite and comparable manner. $\varepsilon_{a,p}$, ΔT and ΔU show a direct interrelation and lead to similar curves. ΔT and ΔU are not related to a defined gauge length and could be helpful to assess the fatigue behaviour of complex components. The electrical resistance and consequently the voltage is furthermore measurable at specimens and components in a load-free state. Thus at real components a proceeding fatigue damage can be detected non-destructively. Cyclic stress-strain, stress-temperature and stress-voltage curves can be described with a modified relationship according to the power law of Morrow. ΔT and ΔU can also be used for a lifetime prediction similar to $\varepsilon_{a,p}$ according to Manson/Coffin.

REFERENCES

[1] Sakamoto, H.; Hirakawa, K.: Prevention of railroad wheel fracture, JSME A 46, 4, 613-619, 2003.

[2] Liu, Z. X.; Gu, H. C.: Failure modes and materials performance of railway wheels, J. Mater. Eng. Perform., 9, 5, 580-584, 2000.

[3] Ekberg, A.; Marais, J.: Effects of imperfections on fatigue initiation in railway wheels, Proc. Inst. Mech. Eng., 214, F, 45-54, 2000.

[4] Walther, F.; Eifler, D.: Microstructure and cyclic deformation behavior of wheel and tire steels in technically relevant heat treatments, Z. Metallkd. 92, 882-887, 2001.

[5] Schelp, M.; Eifler, D.: Evaluation of the HCF-behavior of 42CrMoS4 by means of strain, temperature and electrical measurements, Mater. Sci. Eng. A 319-321, 652-656, 2001.